ACS APPLIED MATERIALS & INTERFACES

Research Article

www.acsami.org

Pressure-Stimulated Synthesis and Luminescence Properties of Microcrystalline $(Lu,Y)_3Al_5O_{12}:Ce^{3+}$ Garnet Phosphors

Victor V. Atuchin,[*,†,‡,§] Nina F. Beisel,[∥,⊥] Eugeniy N. Galashov,[#] Egor M. Mandrik,[#] Maxim S. Molokeev,[▽,○] Alexander P. Yelisseyev,[◆] Alexey A. Yusuf,[*,#] and Zhiguo Xia[*,¶]

[†]Laboratory of Optical Materials and Structures, Institute of Semiconductor Physics, Siberian Branch of the Russian Academy of Sciences, Novosibirsk 630090, Russia

[‡]Functional Electronics Laboratory, Tomsk State University, Tomsk 634050, Russia

[§]Laboratory of Semiconductor and Dielectric Materials, Novosibirsk State University, Novosibirsk 630090, Russia

[∥]Analytical Laboratory, Nikolaev Institute of Inorganic Chemistry, Siberian Branch of the Russian Academy of Sciences, Novosibirsk 630090, Russia

[⊥]Department of Natural Sciences, Novosibirsk State University, Novosibirsk 630090, Russia

[#]Department of Applied Physics, Novosibirsk State University, Novosibirsk 630090, Russia

[▽]Laboratory of Crystal Physics, Kirensky Institute of Physics, Siberian Branch of the Russian Academy of Sciences, Krasnoyarsk 660036, Russia

[○]Department of Physics, Far Eastern State Transport University, Khabarovsk 680021, Russia

[◆]Laboratory of High Pressure Minerals and Diamond Deposits, Institute of Geology and Mineralogy, Siberian Branch of the Russian Academy of Sciences, Novosibirsk 630090, Russia

[¶]School of Materials Sciences and Engineering, University of Science and Technology Beijing, Beijing 100083, China

Supporting Information

ABSTRACT: The $Lu_{2.98}Ce_{0.01}Y_{0.01}Al_5O_{12}$ and $Y_{2.99}Ce_{0.01}Al_5O_{12}$ phosphors were synthesized by solid state reaction at temperature 1623 K and pressure 1.5×10^7 Pa in (95% N_2 + 5% H_2) atmosphere. Under the conditions, the compounds crystallize in the form of isolated euhedral partly faceted microcrystals ~19 μm in size. The crystal structures of the $Lu_{2.98}Ce_{0.01}Y_{0.01}Al_5O_{12}$ and $Y_{2.99}Ce_{0.01}Al_5O_{12}$ garnets have been obtained by Rietveld analysis. The photoluminescence (PL) and X-ray excited luminescence (XL) spectra obtained at room temperature indicate broad asymmetric bands with maxima near 519 and 540 nm for $Y_{2.99}Ce_{0.01}Al_5O_{12}$ and $Lu_{2.98}Ce_{0.01}Y_{0.01}Al_5O_{12}$, respectively. The light source was fabricated using the powder $Lu_{2.98}Ce_{0.01}Y_{0.01}Al_5O_{12}$ phosphor and commercial blue-emitting n-UV LED chips (λ_{ex} = 450 nm). It is found that the CIE chromaticity coordinates are (x = 0.388, y = 0.563) with the warm white light emission correlated color temperature (CCT) of 6400 K and good luminous efficiency of 110 lm/W.

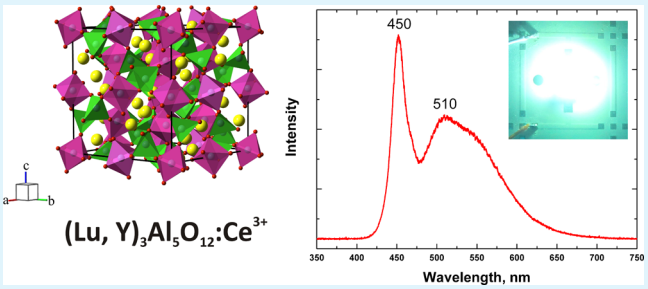

KEYWORDS: *synthesis, pressure, garnet, structure, luminescence, phosphor*

1. INTRODUCTION

Garnet crystals with general composition $A_3B_5O_{12}$ (A = Y or rare-earth element; B = Al, Ga) are of great importance in modern photonics and laser technology.[1−5] The garnet-type materials crystallize in the cubic structure, space group $Ia\bar{3}d$, that excludes the anisotropy of physical properties. As an example, the $Gd_3Al_5O_{12}$ structure is shown in Figure 1.[6,7] The structure is a symmetrical framework formed by alternating sequences of AlO_4 tetrahedra and AlO_6 octahedra with Gd^{3+} ions in the cavities. The garnet structure is thermally and chemically stable, and it can accommodate high doping levels for rare-earth elements by substitution at the A positions. Due to a unique combination of physical and chemical properties, garnet crystals are classified among the best host materials for rare-earth dopants.[3,8−12] However, as it was shown for several A_2O_3−B_2O_3 systems, the garnet phases typically form at high temperatures.[13−16] For this reason, the efficient garnet crystal growth by Czochralski method is possible from iridium crucibles and in a special atmosphere; platinum can be applied

Received: September 8, 2015
Accepted: November 6, 2015
Published: November 6, 2015

DOI: 10.1021/acsami.5b08411
ACS Appl. Mater. Interfaces 2015, 7, 26235−26243

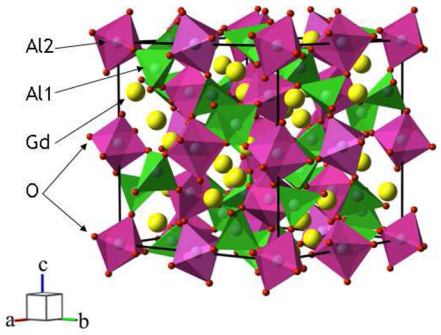

Figure 1. $Gd_3Al_5O_{12}$ crystal structure. The unit cell is outlined. The Al and O lone atoms are omitted for clarity.

only on the flux used to decrease the crystallization temperature.[17−20]

Presently, garnet-based hosts are widely used for phosphor preparation and application in white light-emitting diodes (WLEDs).[21,22] To provide high quantum efficiency of the WLED structure, phosphor particles should possess phase and chemical purity, and narrow size distribution.[23] As it is well-known, such oxide powder products can be prepared by solid state reaction in the air starting from high-purity initial reagents, when the final compound is governed by the initial powder mixture composition and a selected temperature route.[10,12,24−30] In this method, the homogeneous cation distribution is reached through the atom intergrain diffusion and, at appropriate temperatures, a long annealing time is typically needed for crystal lattice stabilization. With regard to the aluminum-garnet-based phosphor formation, the solid state reaction synthesis is commonly performed at as high temperature as T = 1673−1793 K.[10,12,31−34] Evidently, it is desirable to decrease the working temperature needed for garnet-host phosphor crystallization. Thus, the present study is aimed at the garnet-type compound synthesis under pressure stimulation that is a promising way to enhance atom diffusion. The $Y_3Al_5O_{12}$- and $Lu_3Al_5O_{12}$-based phosphors are selected as the representative garnet compounds. For high luminescent efficiency, the phosphor particles should possess high crystallinity, high phase purity, and a low surface defect level. Furthermore, to increase the phosphor brightness and efficiency, sphere-shaped nonaggregated particles are preferable, as compared to irregular-shaped particles. Thus, the synthesis conditions should be optimized for spherical garnet microcrystal preparation.

2. SYNTHESIS AND CHARACTERIZATION

2.1. Sample Synthesis. High-quality oxides Lu_2O_3 (99.9999%, Yeemei Share Ltd., Guangdong, China), Y_2O_3 (99.999%, Yeemei Share), Al_2O_3 (99.99%, Guangzhou Jiechuang Trading Co., China), and CeO_2 (99.99%, Ganzhou Rare Earth, China) were taken as starting reagents. Nominal compositions $Lu_{2.98}Ce_{0.01}Y_{0.01}Al_5O_{12}$ and $Y_{2.99}Ce_{0.01}Al_5O_{12}$ were weighed and mixed in a shaker-mixer SHLM-5 (Applied Mechanics Agency Ltd., St. Petersburg, Russia) for 15 min. Then, the mixed compositions were inserted into alumina crucibles and annealed in the furnace equipped by graphite heaters working up to 1800 °C. The powder mixture was inserted into a crucible without compaction to reduce agglomeration and residual strains in the final product.[35,36] After the sample insertion, the furnace chamber was evacuated up to the residual pressure of 10^{-2} Pa. This stage was needed for air removal from the chamber and particle surface degassing. Then, the chamber was filled with gas in the mixture of 95% N_2 + 5% H_2 by pumping up to pressure 10^5 Pa, and the temperature was increased. When the temperature reached the level of 1623 K, the pressure was increased additionally up to 1.5×10^7 Pa, and, at these conditions, the sample was annealed for 5 h. Under the combination of the temperature and pressure, in accordance to available experimental results,[37] the transition from cubic to monoclinic modification may start in Y_2O_3 sesquioxide, and this induces a drastic atomic disorder stimulating diffusion process. Then, the pressure was decreased to 10^{-2} Pa, and the heat treatment was continued for an extra 5 h. As it is well-known, in solids, the diffusion coefficients decrease with pressure increase.[38−40] For this reason, the finishing stage of the high-temperature treatment was carried out at low pressure. As it is believed, this should increase the microcrystal homogeneity. Finally, the heaters were switched off, and the furnace with the sample was cooled at the rate of 80−100 grad/h to room temperature. After the cooling stage, the sample was removed from the chamber. The samples were annealed individually. The final powder products were of bright yellow color with a light tint difference. There was no postsynthesis treatment or cleaning.

2.2. Experimental Methods. The powder diffraction data of $Lu_{2.98}Ce_{0.01}Y_{0.01}Al_5O_{12}$ and $Y_{2.99}Ce_{0.01}Al_5O_{12}$ for Rietveld analysis were collected at room temperature with a Bruker D8 ADVANCE powder diffractometer (Cu Kα radiation) and linear VANTEC detector. The step size of 2θ was 0.016°, and the counting time was 1 s/step. The Rietveld refinement was performed using package TOPAS 4.2.[41] The particle morphology was observed using TM-1000 (Hitachi Science Systems Ltd., Tokyo, Japan). The particle size distribution was carried out using a Microsizer-210a (Scientific Instruments, St. Petersburg, Russia) device working at λ = 0.6328 μm.

The rare-earth-element contents in their oxides and garnet crystals, as well as other general components of crystals, were determined using atomic emission spectrometry (AES). The samples were carefully mixed with a graphite spectrochemical buffer (C + 4% NaCl), and the mixtures were put into the crater of a graphite electrode (anode) of the direct-current arc (DCA) working at current I = 13.5 A.[42−44] The emission spectra were measured by a diffraction spectrograph PGS-2 (Carl Zeiss, Jena, Germany) with diffraction grating of 650 lines/mm, the spectral resolution being 0.74 nm/mm. The spectrograph was equipped with a Pulse Arc supply source Fareball FB-25 and multichannel analyzer MAES (both from VMK-Optoelektronika, Novosibirsk, Russia) intended for recording emission spectra, as well for results processing by computer program ATOM. For the results confirmation, the mass spectrometric analysis was employed additionally with the use of the double focusing laser mass spectrometer EMAL-2 (SELMI, Sumy, Ukraine) working in the Mattauch-Herzog geometry.[45,46]

The photoluminescence spectra at T = 300 K were measured using a confocal microRaman spectrometer (Horiba), and, in this case, the He−Cd laser (λ = 325 nm) was taken as an excitation source. The powder sample was prepared as a 1 mm thick layer, and excitation was carried out by a focused laser beam of 10 μm in diameter. Besides, the emission spectra were measured comparatively at T = 80 and 300 K under the excitation by the third harmonic of a YAG:Nd laser (λ = 355 nm). The transmission (absorption) spectra were recorded over the spectral range of 200−600 nm. A 50 W incandescent and 25 W deuterium lamps were taken as the light sources, whereas a diffraction monochromator MDR2 (LOMO Ltd., St. Petersburg, Russia) and photomultiplier FEU100 (Moscow Electrolamp Plant, Russia) were used to detect the transmitted light. The spectral resolution of monochromator MDR2 was 2 nm. For the transmission measurements, each sample was pressed in a tablet with the diameter of 3 mm and 0.5 mm in thickness. The spectra of X-ray excited luminescence (XL) were obtained with a monochromator MDR2 at T = 300 K at the excitation from a 1 kW table X-ray setup URS 1.0.

3. RESULTS AND DISCUSSION

The XRD patterns are shown in Figure 2. Almost all peaks were successfully indexed by a cubic cell (space group $Ia\bar{3}d$) with cell parameters close to those of $Y_3Al_5O_{12}$.[47] Therefore, the crystal structure of $Y_3Al_5O_{12}$ was taken as the starting model for

DOI: 10.1021/acsami.5b08411
ACS Appl. Mater. Interfaces 2015, 7, 26235−26243

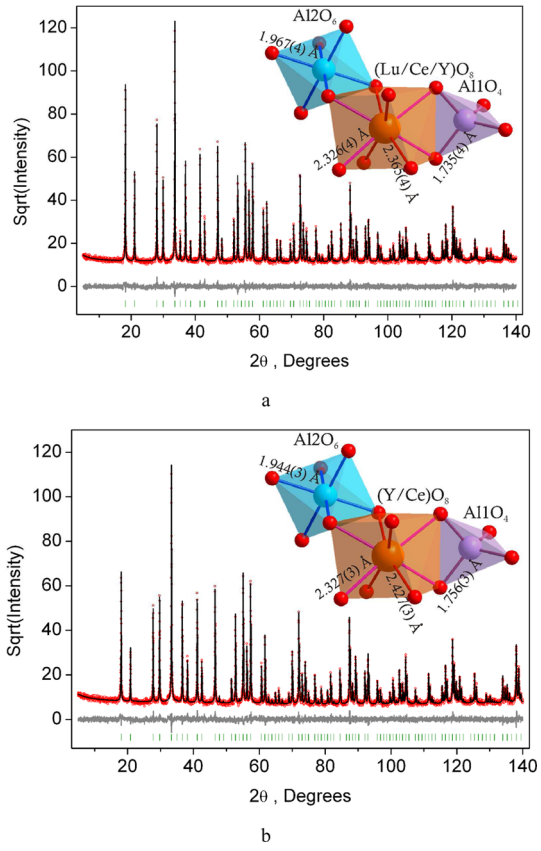

Figure 2. Difference profile plot of (a) $Lu_{2.98}Ce_{0.01}Y_{0.01}Al_5O_{12}$ and (b) $Y_{2.99}Ce_{0.01}Al_5O_{12}$: red dots, experimental pattern (Y_{obs}); black line, calculated pattern (Y_{calc}); gray line, difference ($Y_{obs} - Y_{calc}$); green sticks, main Bragg peaks.

Rietveld refinement of both prepared garnet samples. The Y^{3+} ion site was supposed to be occupied by the corresponding rare-earth-type ions (Lu, Y, Ce) with a fixed occupation according to the nominal compositions. The refinements were stable and gave low *R*-factors, as shown in Table 1 and Figure 2.

Table 1. Main Parameters of Processing and Refinement of the Samples

compound	$Y_{2.99}Ce_{0.01}Al_5O_{12}$	$Lu_{2.98}Ce_{0.01}Y_{0.01}Al_5O_{12}$
space group	$Ia\bar{3}d$	$Ia\bar{3}d$
a, Å	12.01291(3)	11.91706(4)
V, Å^3	1733.58(1)	1692.42(2)
Z	8	8
2θ interval, deg	5−140	5−140
no. of reflcns	143	141
no. of refined params	33	33
R_{wp}, %	11.73	8.23
R_p, %	9.25	6.51
R_{exp}, %	8.74	6.56
χ^2	1.34	1.25
R_B, %	4.14	3.21

The refinement results strongly confirm that the final powder composition is in close relation with the nominal composition for each sample. The atom coordinates are given in Table 2. The doping-element content determination by DCA-AES method yields the $Lu_{2.981}Ce_{0.012}Y_{0.0095}Al_5O_{12}$ and $Y_{2.987}Ce_{0.012}Al_5O_{12}$ compositions, and the values, within possible error ranges, practically coincide with the nominal compositions. This is in good relation to the XRD analysis results.

As it is evident from the bond length comparison, the transition from ($Lu_{2.98}Ce_{0.01}Y_{0.01}$) to ($Y_{2.99}Ce_{0.01}$) in the A-site content results in a volume decrease of aluminum octahedra and tetrahedra. Comparatively, the volumes of [AO_8] polyhedra increase. Thus, the trends are opposite. Before synthesis, it can be reasonably supposed that the unit cell volume of $Y_{2.99}Ce_{0.01}Al_5O_{12}$ is to be bigger than that of $Lu_{2.98}Ce_{0.01}Y_{0.01}Al_5O_{12}$ because the ionic radius of Y^{3+} is higher than that of Lu^{3+}.[48] It is interesting to compare the cell volumes of these two doped garnets with the earlier results reported for other aluminum garnets. The dependence of unit cell volume on averaged effective ionic radii (IR) of elements in the A site is shown in Figure 3. The considered aluminum garnet structures are presented in Supporting Information Table 1S.[6,47,49−52] The linear cell volume increase on the IR(A) increase is evident, and the points obtained in the present study are very close to the general curve. This additionally confirms the structural quality of the synthesized samples.

The morphologies of $Y_{2.99}Ce_{0.01}Al_5O_{12}$ and $Lu_{2.98}Ce_{0.01}Y_{0.01}Al_5O_{12}$ products are shown in Figure 4. Under the synthesis conditions, the garnets crystallize as isolated microsized euhedral partly faceted crystals. The size distributions are narrow with a maximum at ∼19 μm. For $Lu_{2.98}Ce_{0.01}Y_{0.01}Al_5O_{12}$, however, lower size components are significant. Thus, it can be concluded, that the synthesis conditions are well-reproducible and the final particle morphology is practically independent of heavy cation selection for the A sites.

The appearance of the faceted shapes indicates that the atom diffusion was active enough to achieve the equilibrium microcrystal shapes for a relatively short annealing time. Previously, a similar effect was detected for several complex molybdates and tungstates where the atom diffusion process is supported by MoO_3 or WO_3 gas phase transport.[25,27,53−56] In the garnets, however, the volatile components are absent and another mechanism for atom exchange activation should be proposed. As it seems, the key factor is the combination of high temperature and pressure. Indeed, cubic rare-earth sesquioxides undergo phase transition to the low symmetry state at a high temperature or pressure, and the cubic phase boundary greatly decreases when the temperature and pressure are applied in combination.[57−59] Besides, similar effects are observed for the Al_2O_3 high-temperature phase transformations.[60−62] Thus, the conditions of the garnet synthesis implemented in the present study may cover the phase transition regions of all of the basic initial oxides. In the vicinity of the phase transition, the atom lattice order is unstable and this drastically enhances the garnet composition homogenization by diffusion.

The photoluminescence (PL) spectra of $Y_{2.99}Ce_{0.01}Al_5O_{12}$ and $Lu_{2.98}Ce_{0.01}Y_{0.01}Al_5O_{12}$ obtained at room temperature under photoexcitation by a 325 nm laser beam are shown in Figure 5. The dominating features are broad asymmetric bands with the maximums near 519 and 540 nm for $Y_{2.99}Ce_{0.01}Al_5O_{12}$ and $Lu_{2.98}Ce_{0.01}Y_{0.01}Al_5O_{12}$, respectively. Besides, two orders weaker components were observed near 406 nm. The PL intensity in the main emission band estimated from the area under the PL curves, is approximately 1.96 times higher for $Lu_{2.98}Ce_{0.01}Y_{0.01}Al_5O_{12}$. The difference in the maximum position is consistent for the unit cell parameters difference of the $Y_{2.99}Ce_{0.01}Al_5O_{12}$ and $Lu_{2.98}Ce_{0.01}Y_{0.01}Al_5O_{12}$ crystals, as shown

DOI: 10.1021/acsami.5b08411
ACS Appl. Mater. Interfaces 2015, 7, 26235−26243

Table 2. Fractional Atomic Coordinates and Isotropic Displacement Parameters (Å^2) of the Samples

	x	y	z	B_{iso}	occ.
		$Y_{2.99}Ce_{0.01}Al_5O_{12}$			
Y	0	0.25	0.125	0.47 (4)	0.9967
Ce	0	0.25	0.125	0.47 (4)	0.0033
Al1	0	0.25	0.375	0.77 (4)	1
Al2	0	0	0	0.43 (5)	1
O	−0.0323 (2)	0.0521 (2)	0.1497 (2)	0.70 (7)	1
		$Lu_{2.98}Ce_{0.01}Y_{0.01}Al_5O_{12}$			
Lu	0	0.25	0.125	0.58 (3)	0.9934
Ce	0	0.25	0.125	0.58 (3)	0.0033
Y	0	0.25	0.125	0.58 (3)	0.0033
Al1	0	0.25	0.375	1.05 (6)	1
Al2	0	0	0	0.53 (7)	1
O	−0.0338 (3)	0.0563 (3)	0.1514 (3)	0.52 (9)	1

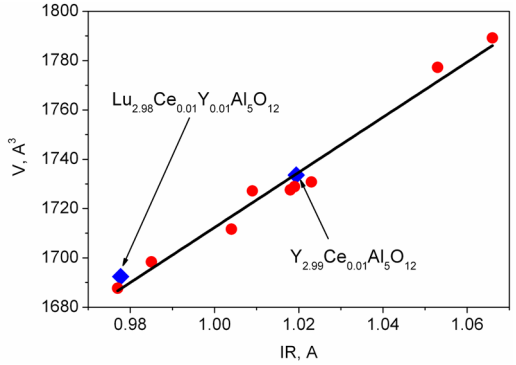

Figure 3. Cell volume dependence on averaged effective rare-earth ion radius in aluminum garnet structures.

in Supporting Information Table 1S. The maximum positions are in the spectral ranges typically observed in the $Y_3Al_5O_{12}$:Ce^{3+} and $Lu_3Al_5O_{12}$:Ce^{3+} phosphors prepared by different methods.[11,12,21,32,63−66] It is known that, in garnet-based phosphors, the increase of structural disorder induces the shift of emission band maximum to longer wavelengths.[67] However, the spectral position of the maximum measured for $Y_{2.99}Ce_{0.01}Al_5O_{12}$ is at comparatively short wavelength, within the possible range in $Y_3Al_5O_{12}$:Ce^{3+} solid solutions, and this indicates that pressure application during annealing provides a high atom ordering in the garnet lattice.

The PL spectra of $Y_{2.99}Ce_{0.01}Al_5O_{12}$ and $Lu_{2.98}Ce_{0.01}Y_{0.01}Al_5O_{12}$ powders, recorded at 355 nm at 300 and 80 K, and the X-ray excited luminescence (XL) spectra are given in Figure 6. Here, at 300 K, the broad bands in XR and PL spectra in Figure 6 are very similar to those in Figure 5. Some shift in the peak position is due to the use of different monochromators. At 80 K, one can distinguish two components in the main emission band for both powders. The results of decomposition into Gaussian components are given in Table 3, where the peak maximum position and the full width at half-maximum level (fwhm) are indicated. The distance between the components is 0.218 and 0.220 eV for $Y_{2.99}Ce_{0.01}Al_5O_{12}$ and $Lu_{2.98}Ce_{0.01}Y_{0.01}Al_5O_{12}$, respectively. The comparison of spectra 1 and 2 in Figure 6c,d shows that the doublet components become more intense and narrower on temperature decreases. However, the integral PL intensity does not change. Thus, there is no PL quenching in the temperature range of 80−300 K in $Y_{2.99}Ce_{0.01}Al_5O_{12}$ and $Lu_{2.98}Ce_{0.01}Y_{0.01}Al_5O_{12}$. Indeed, PL quenching onset was

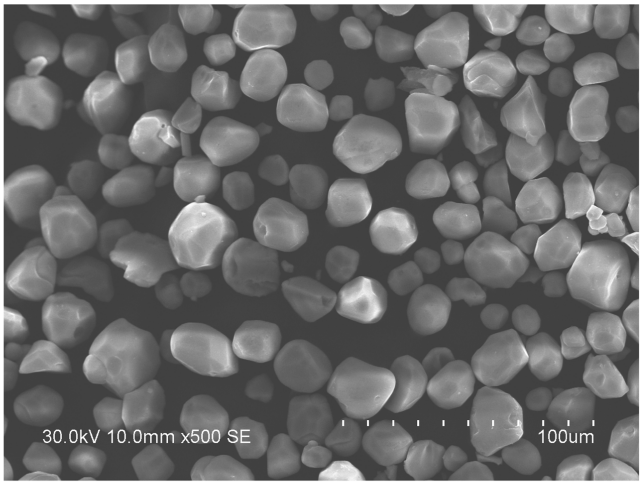

a

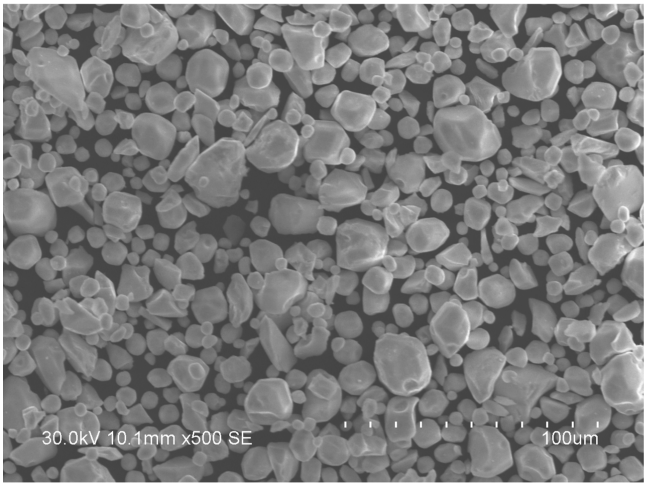

b

Figure 4. SEM patterns obtained from (a) $Y_{2.99}Ce_{0.01}Al_5O_{12}$ and (b) $Lu_{2.98}Ce_{0.01}Y_{0.01}Al_5O_{12}$.

observed at the temperature of about 600 and 700 K for $Y_{2.99}Ce_{0.01}Al_5O_{12}$ and $Lu_{2.98}Ce_{0.01}Y_{0.01}Al_5O_{12}$, respectively.[68]

The transmission and luminescence excitation spectra for $Y_{2.99}Ce_{0.01}Al_5O_{12}$ and $Lu_{2.98}Ce_{0.01}Y_{0.01}Al_5O_{12}$ powders, prepared as translucent tablets, are given in Figure 7. One can see that the powders become transparent at a wavelength above 500 nm, whereas, at shorter wavelengths, it is possible to distinguish

DOI: 10.1021/acsami.5b08411
ACS Appl. Mater. Interfaces 2015, 7, 26235−26243

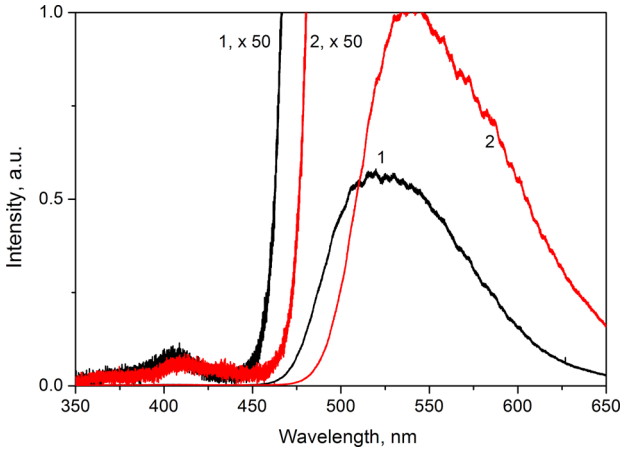

Figure 5. PL spectra of (1) $Y_{2.99}Ce_{0.01}Al_5O_{12}$ and (2) $Lu_{2.98}Ce_{0.01}Y_{0.01}Al_5O_{12}$ recorded under 325 nm excitation by a He–Cd laser at 300 K.

two intense absorption bands at about 340 and 450 nm. The PLE spectra were measured for 530 and 570 nm emissions. These spectra are similar, and we show only the PLE spectra for 570 nm PL. There are three main bands in the PLE spectra. For $Y_{2.99}Ce_{0.01}Al_5O_{12}$, they are located near 230, 340, and 444 nm, whereas the later band is shifted about 15 nm to longer wavelengths in the case of $Lu_{2.98}Ce_{0.01}Y_{0.01}Al_5O_{12}$. There is a good correlation between the absorption and PLE spectra for $Y_{2.99}Ce_{0.01}Al_5O_{12}$ and $Lu_{2.98}Ce_{0.01}Y_{0.01}Al_5O_{12}$. Since the bandgap is 6.96 eV for pure YAG[69] and about 8 eV for pure LuAG,[70] both powders should be transparent in the spectral range under examination. Thus, all spectroscopic features in the transmission and PLE spectra may be associated with Ce^{3+} in the garnet lattice.[65,66]

Table 3. Results of the Low-Temperature PL Spectra Decomposition into Gaussian Components for $Y_{2.99}Ce_{0.01}Al_5O_{12}$ and $Lu_{2.98}Ce_{0.01}Y_{0.01}Al_5O_{12}$ (T = 80 K)

	$Y_{2.99}Ce_{0.01}Al_5O_{12}$			$Lu_{2.98}Ce_{0.01}Y_{0.01}Al_5O_{12}$		
	peak max position			peak max position		
	nm	eV	fwhm, eV	nm	eV	fwhm, eV
1	499.8	2.480	0.169	523.0	2.370	0.182
2	547.9	2.262	0.234	576.5	2.150	0.225

Cerium is an n-type dopant in YAG as the cerium 4f donor state lies about 1.5 eV above the valence band and the empty cerium 5d state is about 2.5 eV higher.[70,71] However, in an oxidized crystal, cerium may appear in its 4+ valence state making the Fermi energy fall below the cerium band creating a p-type environment in the crystal.[71] A simplistic energy level diagram of cerium in YAG is shown in Figure 8. The dominant emission band is attributed to the 5d → 4f optical transition in the Ce^{3+} ions.[21,22] A doublet structure of the main band is due to the splitting of the ^2F ground state to $^2F_{5/2}$ and $^2F_{7/2}$ states by spin–orbit (SO) coupling. The lower ground state is $^2F_{5/2}$. The typical SO splitting of 2000 cm^{-1} is observed in the emission spectrum due to transitions from the lowest $5d_1$ state to both ^2F_J states. For $Y_{2.99}Ce_{0.01}Al_5O_{12}$ and $Lu_{2.98}Ce_{0.01}Y_{0.01}Al_5O_{12}$, the SO splittings are 1761 and 1774 cm^{-1} (Table 3), respectively. As to the 340 nm band in the absorption/PLE spectra, it was associated with a transition from the ground ^2F state to the conduction band (Figure 8), whereas emission in the 380–400 nm band corresponds to reverse radiative transition from the conduction band bottom to the ^2F ground state. At 340 nm illumination, the Ce^{3+} center is ionized

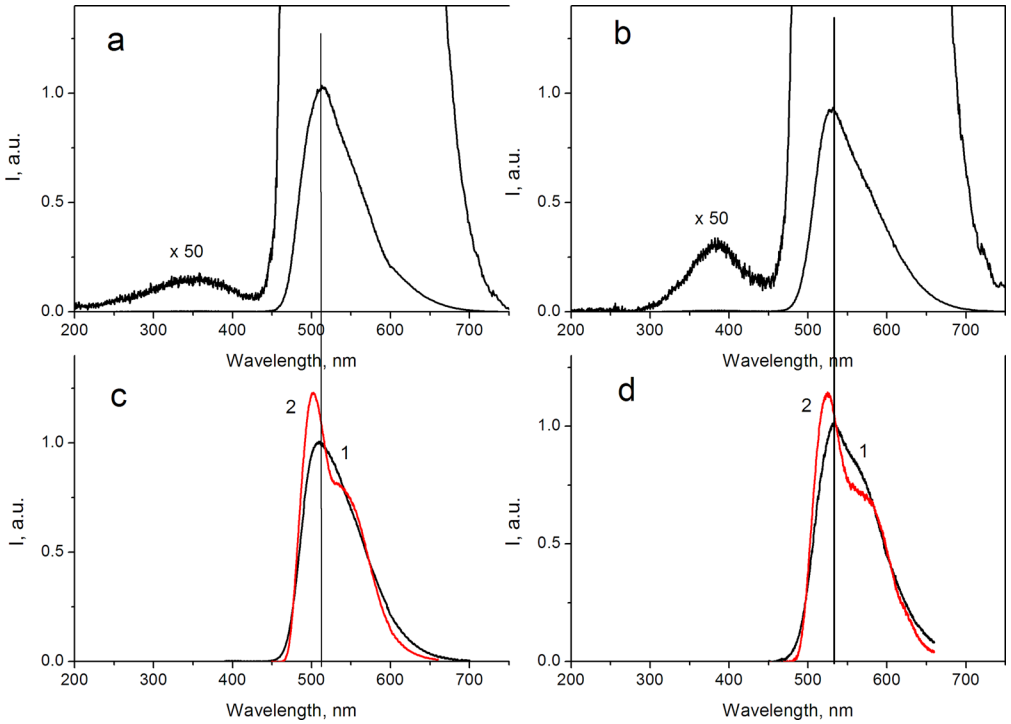

Figure 6. (a, b) The XL and (c, d) PL spectra carried out from (a, c) $Y_{2.99}Ce_{0.01}Al_5O_{12}$ and (b, d) $Lu_{2.98}Ce_{0.01}Y_{0.01}Al_5O_{12}$ phosphors. The XL spectra are shown also at the ×50 magnification. PL was excited by a 355 nm laser beam. PL spectra 1 and 2 were recorded at 300 and 80 K, respectively. The dotted lines show maximum positions at 300 K in XL and PL spectra.

DOI: 10.1021/acsami.5b08411
ACS Appl. Mater. Interfaces 2015, 7, 26235–26243

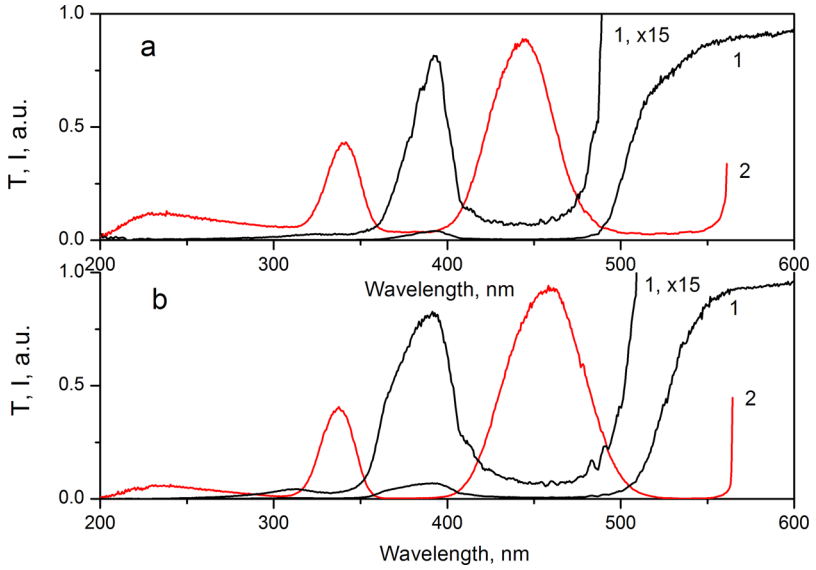

Figure 7. (1) Transmission spectra and (2) PLE spectra recorded for the tablets prepared from (a) $Y_{2.99}Ce_{0.01}Al_5O_{12}$ and (b) $Lu_{2.98}Ce_{0.01}Y_{0.01}Al_5O_{12}$ powders. The transmission spectra are shown also with the ×15 magnification. The PLE spectra were recorded for the 570 nm emission, T = 300 K.

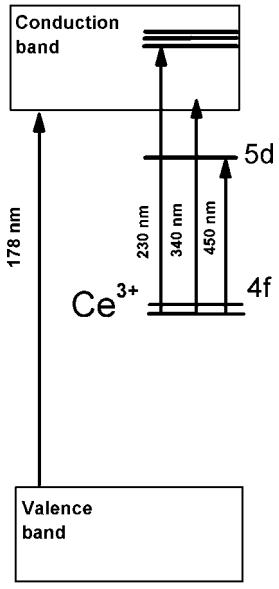

Figure 8. Simplified energy level diagram of Ce^{3+} in garnets.

and it transforms to the Ce^{4+} state.[72,73] The appearance of Ce^{4+} ions in YAG is usually associated with thermal processing. During high-temperature annealing in an oxidizing atmosphere, transformation $Ce^{3+} \rightarrow Ce^{4+}$ is possible.[72,73] A broad band near 230 nm is supposed to be a result of electron transition to the higher lying 5d states of Ce^{3+} located deeper in the conduction band (Figure 8).

To evaluate the potential of the garnet-based phosphors prepared under pressure-stimulated annealing, the light source is fabricated using powder $Lu_{2.98}Ce_{0.01}Y_{0.01}Al_5O_{12}$ phosphor and commercial blue-emitting n-UV LED chips (λ_{ex} = 450 nm). The device fabrication technique can be found elsewhere.[21,74,75] The fabricated *w*-LEDs lamp and their emission spectrum are shown in Figure 9. The blue sharp band (λ_{ex} = 450 nm) appeared due to LED emission, and the greenish-yellow wide band (λ_{ex} = 510 nm) is induced by $Lu_{2.98}Ce_{0.01}Y_{0.01}Al_5O_{12}$ phosphor. The turned on *w*-LEDs lamp is shown in the inset of

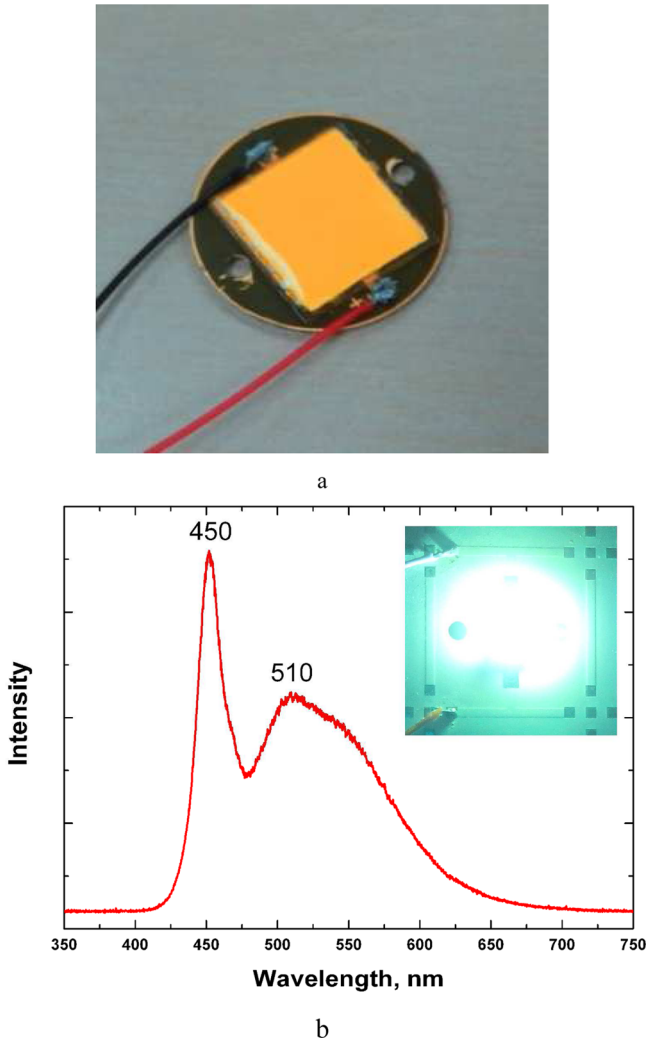

Figure 9. (a) Photograph of the *w*-LED lamp package and (b) emission spectrum of the *w*-LED lamp based on $Lu_{2.98}Ce_{0.01}Y_{0.01}Al_5O_{12}$ phosphor.

DOI: 10.1021/acsami.5b08411
ACS Appl. Mater. Interfaces 2015, 7, 26235−26243

Figure 9b. It is found that the CIE chromaticity coordinates are (x = 0.388, y = 0.563) with the warm white light emission correlated color temperature (CCT) of 6400 K and good luminous efficiency of 110 lm/W. For comparison, the CIE chromaticity coordinates obtained for w-LEDs lamp fabricated with the $Y_{2.99}Ce_{0.01}Al_5O_{12}$ phosphor are (x = 0.395, y = 0.360) with the CCT of 5000 K and luminous efficiency of 120 lm/W. Thus, the $Y_{2.99}Ce_{0.01}Al_5O_{12}$ and $Lu_{2.98}Ce_{0.01}Y_{0.01}Al_5O_{12}$ phosphors are promising for application in w-LEDs.

4. CONCLUSIONS

The results of this study testify that high-quality garnet phosphors can be prepared by solid state reaction at a comparatively low temperature under pressure stimulation. The reaction of the garnet compound formation is finished in a short time; the final phosphor particles are partly faceted, and that indicates low surface defect concentration. High structural quality of the garnet powders is confirmed by XRD analysis. There is no noticeable chemical composition variation during high-temperature synthesis. The spectroscopic parameters of $Y_{2.99}Ce_{0.01}Al_5O_{12}$ and $Lu_{2.98}Ce_{0.01}Y_{0.01}Al_5O_{12}$ garnets are in good relation to those early reported for the garnet compounds prepared by traditional methods. Generally, the experiment reveals that the temperature/pressure combination is a promising way to stimulate atom interdiffusion, and this method should be tested for other oxide materials.

■ ASSOCIATED CONTENT

Supporting Information

Table 1S. The Supporting Information is available free of charge on the ACS Publications website at DOI: 10.1021/acsami.5b08411.

Crystallographic information for $Y_{2.99}Ce_{0.01}Al_5O_{12}$ garnet (CIF)

Crystallographic information for $Lu_{2.98}Ce_{0.01}Y_{0.01}Al_5O_{12}$ garnet (CIF)

Table 1S listing garnet unit cell volumes (PDF)

■ AUTHOR INFORMATION

Corresponding Authors

*(V.V.A.) Phone: +7 (383) 3308889. E-mail: atuchin@isp.nsc.ru.

*(A.A.Y.) Phone: +7 913 9875434. E-mail: chessplanet86@yandex.ru.

*(Z.X.) Phone: +86 (10) 82377955. E-mail: xiazg@ustb.edu.cn.

Notes

The authors declare no competing financial interest.

■ ACKNOWLEDGMENTS

This work was partly supported by the National Natural Science Foundations of China (Grant Nos. 51272242 and 51511130035) and the Russian Foundation for Basic Research (Grant No. 15-52-53080 GFEN_a). V.V.A. was partly supported by the Ministry of Education and Science of the Russian Federation.

■ REFERENCES

(1) Jüstel, T.; Nikol, H.; Ronda, C. New Development in the Field of Luminescent Materials for Lighting and Displays. *Angew. Chem., Int. Ed.* **1998**, *37*, 3084−3103.

(2) Huber, G.; Kränkel, C.; Petermann, K. Solid-State Lasers: Status and Future. *J. Opt. Soc. Am. B* **2010**, *27*, B93−B105.

(3) Speghini, A.; Piccinelli, F.; Bettinelli, M. Synthesis, Characterization and Luminescence Spectroscopy of Oxide Nanopowders Activated with Trivalent Lanthanide Ions: The Garnet Family. *Opt. Mater.* **2011**, *33*, 247−257.

(4) Chen, F. Micro- and Submicrometric Waveguiding Structures in Optical Crystals Produced by Ion Beams for Photonic Applications. *Laser Photon. Rev.* **2012**, *6*, 622−640.

(5) Sanghera, J.; Kim, W.; Villalobos, G.; Shaw, B.; Baker, C.; Frantz, J.; Sadowski, B.; Aggarwal, I. Ceramic Laser Materials: Past and Present. *Opt. Mater.* **2013**, *35*, 693−699.

(6) Euler, F.; Bruce, J. A. Oxygen Coordinates of Compounds with Garnet Structure. *Acta Crystallogr.* **1965**, *19*, 971−978.

(7) Ozawa, T. C.; Kang, S. J. Balls&Sticks: Easy-to-Use Structure Visualization and Animation Program. *J. Appl. Crystallogr.* **2004**, *37*, 679.

(8) Boyer, J. C.; Vetrone, F.; Capobianco, J. A.; Speghini, A.; Bettinelli, M. Yb^{3+} Ion as a Sensitizer for the Upconversion Luminescence in Nanocrystalline $Gd_3Ga_5O_{12}$:Ho^{3+}. *Chem. Phys. Lett.* **2004**, *390*, 403−407.

(9) Aleksandrovsky, A. S.; Arkhipkin, V. G.; Bezmaternykh, L. N.; Gudim, I. A.; Krylov, A. S.; Vagizov, F. Origin of Color Centers in the Flux-Grown Europium Gallium Garnet. *J. Appl. Phys.* **2008**, *103*, 083102.

(10) Luo, Y.; Xia, Z. G. Effect of Al/Ga Substitution on Photoluminescence and Phosphorescence Properties of Garnet-Type $Y_3Sc_2Ga_{3-x}Al_xO_{12}$:$Ce^{3+}$ Phosphor. *J. Phys. Chem. C* **2014**, *118*, 23297−23305.

(11) Lojpur, V.; Egelja, A.; Pantić, J.; Đorđević, V.; Matović, B.; Dramićanin, M. D. $Y_3Al_5O_{12}$:Re^{3+} (Re = Ce, Eu, and Sm) Nanocrystalline Powders Prepared by Modified Glycine Combustion Method. *Sci. Sintering* **2014**, *46*, 75−82.

(12) Zhou, W.; Ma, X. X.; Zhang, M. L.; Luo, Y.; Xia, Z. G. Synthesis and Photoluminescence Properties of Green-Emitting $Lu_3(Al,Sc)_5O_{12}$:Ce^{3+} Phosphor. *Ceram. Int.* **2015**, *41*, 7140−7145.

(13) Wu, P.; Pelton, A. D. Coupled Thermodynamic-Phase Diagram Assessment of the Rare Earth Oxide-Aluminium Oxide Binary Systems. *J. Alloys Compd.* **1992**, *179*, 259−287.

(14) Udalov, Yu. P.; Rakhmankulov, R. M.; Chemekova, T. Yu.; Belousova, O. L. Crystallization and Phase Equilibria in the Tb_2O_3-Ga_2O_3 System. *Glass Phys. Chem.* **2003**, *29*, 200−201.

(15) Han, Y. H.; Nagata, M.; Uekawa, N.; Kakegawa, K. Eutectic Al_2O_3-$GdAlO_3$ Composite Consolidated by Combined Rapid Quenching and Spark Plasma Sintering Technique. *Br. Ceram. Trans.* **2004**, *103*, 219−222.

(16) Popova, V. F.; Petrosyan, A. G.; Tugova, E. A.; Romanov, D. P.; Gusarov, V. V. Y_2O_3-Ga_2O_3 Phase Diagram. *Russ. J. Inorg. Chem.* **2009**, *54*, 624−629.

(17) Bezmaternykh, L. N.; Mashchenko, V. G.; Sokolova, N. A.; Temerov, V. L. Growth of Iron Garnet Single Crystals on a Rotating Carrier from BaO/B_2O_3 Fluxes. *J. Cryst. Growth* **1984**, *69*, 407−413.

(18) Kimura, H.; Miyazaki, A. Optical Properties of Czochralski Grown Rare-Earth Garnet Single Crystals in Solid Solution. *J. Cryst. Growth* **2003**, *250*, 251−255.

(19) Zhuravleva, M.; Friedrich, S.; Melcher, C. L. Praseodymium Valemce Determination in Lu_2SiO_5, Y_2SiO_5, and $Lu_3Al_5O_{12}$ Scintillators by X-ray Absorption Spectroscopy. *Appl. Phys. Lett.* **2012**, *101*, 101902.

(20) Wu, Y. T.; Ren, G. H. Crystal Growth, Structure, Optical and Scintillation Properties of Ce^{3+}-Doped $Tb_{2.2}Lu_{0.8}Al_5O_{12}$ Single Crystals. *CrystEngComm* **2013**, *15*, 4153−4161.

(21) Chen, L.; Lin, C.-C.; Yeh, C.-W.; Liu, R.-S. Light Converting Inorganic Phosphors for White Light-Emitting Diodes. *Materials* **2010**, *3*, 2172−2195.

(22) Dorenbos, P. Electronic Structure and Optical Properties of the Lanthanide Activated $RE_3(Al_{1-x}Ga_x)_5O_{12}$ (RE = Gd, Y, Lu) Garnet Compounds. *J. Lumin.* **2013**, *134*, 310−318.

(23) Shang, M. M.; Li, C. X.; Lin, J. How to Produce White Light in a Single-Phase Host? *Chem. Soc. Rev.* **2014**, *43*, 1372−1386.

DOI: 10.1021/acsami.5b08411
ACS Appl. Mater. Interfaces 2015, 7, 26235−26243

(24) Atuchin, V. V.; Grivel, J.-C.; Korotkov, A. S.; Zhang, Z. M. Electronic Parameters of $Sr_2Nb_2O_7$ and Chemical Bonding. *J. Solid State Chem.* **2008**, *181*, 1285−1291.
(25) Atuchin, V. V.; Gavrilova, T. A.; Grivel, J. C.; Kesler, V. G. Electronic Structure of Layered Ferroelectric High-k Titanate $La_2Ti_2O_7$. *J. Phys. D: Appl. Phys.* **2009**, *42*, 035305.
(26) Atuchin, V. V.; Chimitova, O. D.; Gavrilova, T. A.; Molokeev, M. S.; Kim, S.-J.; Surovtsev, N. V.; Bazarov, B. G. Synthesis, Structural and Vibrational Properties of Microcrystalline $RbNd(MoO_4)_2$. *J. Cryst. Growth* **2011**, *318*, 683−686.
(27) Atuchin, V. V.; Bazarov, B. G.; Gavrilova, T. A.; Grossman, V. G.; Molokeev, M. S.; Bazarova, Zh.G. Preparation and Structural Properties of Nonlinear Optical Borates $K_{2(1-x)}Rb_{2x}Al_2B_2O_7$, $0 < x < 0.75$. *J. Alloys Compd.* **2012**, *515*, 119−122.
(28) Alekseev, E. V.; Felbinger, O.; Wu, S.; Malcherek, T.; Depmeier, W.; Modolo, G.; Gesing, T. M.; Krivovichev, S. V.; Suleimanov, E. V.; Gavrilova, T. A.; Pokrovsky, L. D.; Pugachev, A. M.; Surovtsev, N. V.; Atuchin, V. V. $K[AsW_2O_9]$, the First Member of the Arsenate-Tungsten Bronze Family: Synthesis, Structure, Spectroscopic and Non-Linear Optical Properties. *J. Solid State Chem.* **2013**, *204*, 59−63.
(29) Ji, H. P.; Huang, Z. H.; Xia, Z. G.; Molokeev, M. S.; Atuchin, V. V.; Fang, M.H.; Huang, S. F. New Yellow-Emitting Whitlockite-Type Structure $Sr_{1.75}Ca_{1.25}(PO_4)_2:Eu^{2+}$ Phosphor for Near-UV Pumped White Light-Emitting Devices. *Inorg. Chem.* **2014**, *53*, 5129−5135.
(30) Ji, H. P.; Huang, Z. H.; Xia, Z. G.; Molokeev, M. S.; Chen, M. G.; Atuchin, V. V.; Fang, M. H.; Liu, Y.; Wu, X. W. Phase Transformation in $Ca_3(PO_4)_2:Eu^{2+}$ via the Controlled Quenching and Increased Eu^{2+} Content: Identification of New Cyan-Emitting α-$Ca_3(PO_4)_2:Eu^{2+}$ Phosphor. *J. Am. Ceram. Soc.* **2015**, *98*, 3280−3284.
(31) Hattori, T.; Nishiyama, S.; Fukuda, M.; Iwadate, Y. Preparation of Garnet-Type $Gd_3Al_5O_{12}$ Powders by an Amorphous Citrate Process. *Nippon Seramikkusu Kyokai Gakujutsu Ronbunshi* **1992**, *100*, 1381−1383.
(32) Huang, S. C.; Wu, J. K.; Hsu, W.-J.; Chang, H. H.; Hung, H. Y.; Lin, C. L.; Su, H.-Y.; Bagkar, N.; Ke, W.-C.; Kuo, H. T.; Liu, R.-S. Particle Size Effect on the Packaging Performance of YAG:Ce Phosphors in White LEDs. *Int. J. Appl. Ceram. Technol.* **2009**, *6*, 465−469.
(33) Wu, Y. T.; Ren, G. H. Effects of Ga/Lu Ratio on the Luminescent Properties of Pr^{3+} Activated $(Gd,Lu)_3Ga_3Al_2O_{12}$. *ECS J. Solid State Sci. Technol.* **2013**, *2*, R49−R55.
(34) Han, G. S.; Song, Y. H.; Kim, D. H.; Lee, M.-J.; Lee, D. G.; Han, S.-H.; Kim, Y. J.; Jung, M.-K.; Yoon, D.-H.; Jung, H. S. Green-Emitting $Lu_3Al_5O_{12}:Ce^{3+}$ Phosphor as a Visible Light Amplifier for Dye-Sensitized Solar Cells. *RSC Adv.* **2015**, *5*, 24737−24741.
(35) Atuchin, V. V.; Gavrilova, T. A.; Grivel, J.-C.; Kesler, V. G. Electronic Structure of Layered Titanate $Nd_2Ti_2O_7$. *Surf. Sci.* **2008**, *602*, 3095−3099.
(36) Atuchin, V. V.; Gavrilova, T. A.; Grivel, J.-C.; Kesler, V. G.; Troitskaia, I. B. Electronic Structure of Layered Ferroelectric High-k Titanate $Pr_2Ti_2O_7$. *J. Solid State Chem.* **2012**, *195*, 125−131.
(37) Yusa, H.; Tsuchiya, T.; Sata, N.; Ohishi, Y. Dense Yttria Phase Eclipsing the A-type Sesquioxide Structure: High-Pressure Experiments and ab initio Calculations. *Inorg. Chem.* **2010**, *49*, 4478−4485.
(38) Aziz, M. J. Thermodynamics of Diffusion Under Pressure and Stress: Relation to Point Defect Mechanism. *Appl. Phys. Lett.* **1997**, *70*, 2810−2812.
(39) Van Orman, J. A.; Grove, T. L.; Shimizu, N. Rare Earth Element Diffusion in Diopside: Influence of Temperature, Pressure, and Ionic Radius, and an Elastic Model for Diffusion in Silicates. *Contrib. Mineral. Petrol.* **2001**, *141*, 687−703.
(40) Van Orman, J. A.; Crispin, K. L. Diffusion in Oxides. *Rev. Mineral. Geochem.* **2010**, *72*, 757−825.
(41) Bruker AXS TOPAS V4: General Profile and Structure Analysis Software for Powder Diffraction Data—User's Manual; Bruker AXS: Karlsruhe, Germany, 2008.
(42) Kozeeva, L. P.; Kameneva, M. Y.; Podberezskaya, N. V.; Naumov, D. Y.; Beizel, N. F.; Fedorov, V. E. Preparation and Characterization of HTSC $LuBa_2Cu_3O_{6+x}$ Single Crystals. *J. Ceram. Process. Res.* **2002**, *3*, 123−127.
(43) Kozeeva, L. P.; Kameneva, M. Yu.; Beizel, N. F.; Fedorov, V. E. Off-Stoichiometric Melt Growth of $LuBa_2Cu_3O_{6+x}$ Crystals. *Inorg. Mater.* **2002**, *38*, 1026−1031.
(44) Kozeeva, L. P.; Podberezskaya, N. V.; Kameneva, M. Yu.; Naumov, D. Yu.; Beizel, N. F.; Blinov, A. G.; Fedorov, V. E. Growth Conditions, Structure, and Composition of Sm123 Crystals. *J. Struct. Chem.* **2005**, *46*, 465−473.
(45) Sysoev, V. I.; Troitsky, D. Yu.; Saprykin, A. I. Analysis of Silicon Carbonitride Films by Laser Mass Spectrometry. *J. Anal. Chem.* **2013**, *68*, 1212−1216.
(46) Petrova, N. I.; Troitskii, D. Yu.; Novoselov, I. I.; Saprykin, A. I. Determination of Chlorine in Bismuth and Bismuth Oxide by Atomic Absorption Spectrometry and Laser Mass Spectrometry. *Inorg. Mater.* **2015**, *51*, 559−562.
(47) Bagdasarov, Kh.S.; Bolotina, N. B.; Kalinin, V. I.; Karyagin, V. F.; Kuz'min, B. V.; Muradyan, L. A.; Ryadnov, S. N.; Uyukin, E. M.; Chernaya, T. S.; Fedorov, E. A.; Chudakov, V. S.; Simonov, V. I. Photoinduced Effects and Real Structure of Crystals of Yttrium Aluminum Garnet. *Kristallografiya* **1991**, *36*, 398−405.
(48) Shannon, R. D. Revised Effective Ionic Radii and Systematic Studies of Interatomic Distances in Halides and Chalcogenides. *Acta Crystallogr., Sect. A: Cryst. Phys., Diffr., Theor. Gen. Crystallogr.* **1976**, *32*, 751−767.
(49) Chernaya, T. S.; Muradyan, L. A.; Rusakov, A. A.; Kaminskii, A. A.; Simonov, V. I. Refinement and Analysis of Atomic Structures of $Er_3Al_5O_{12}$ and $(Y_{2.80}Er_{0.20})Al_5O_{12}$. *Kristallografiya* **1985**, *30*, 72−75.
(50) Chernaya, T. S.; Goreva, T. F.; Akhmetov, S. F.; Loshmanov, A. A.; Muradyan, L. A.; Simonov, V. I. Neutron-Diffraction Refinement of the Atomic Structure of $Y_{2.25}Lu_{0.75}Al_5O_{12}$. *Kristallografiya* **1989**, *34*, 323−326.
(51) Zhang, F. F.; Song, K. X.; Jiang, J.; Wu, S.; Zheng, P.; Huang, Q. M.; Xu, J. M.; Qin, H. B. Improvement of Photoluminescence Properties and Thermal Stability of $Y_{2.9}Ce_{0.1}Al_{5-x}Si_xO_{12}$ Phosphors with Si_3N_4 Addition. *J. Alloys Compd.* **2014**, *615*, 588−593.
(52) Garskaite, E.; Sakirzanovas, S.; Kareiva, A.; Glaser, J.; Meyer, H. J. Synthesis and Structure of Europium Aluminium Garnet (EAG). *Z. Anorg. Allg. Chem.* **2007**, *633*, 990−993.
(53) Troitskaia, I. B.; Gavrilova, T. A.; Gromilov, S. A.; Sheglov, D. V.; Atuchin, V. V.; Vemuri, R. S.; Ramana, C. V. Growth and Structural Properties of α-MoO_3 (010) Microplates with Atomically Flat Surface. *Mater. Sci. Eng., B* **2010**, *174*, 159−163.
(54) Atuchin, V. V.; Chimitova, O. D.; Adichtchev, S. V.; Bazarov, B. G.; Gavrilova, T. A.; Molokeev, M. S.; Surovtsev, N. V.; Bazarova, Zh.G. Synthesis, Structural and Vibrational Properties of Microcrystalline β-$RbSm(MoO_4)_2$. *Mater. Lett.* **2013**, *106*, 26−29.
(55) Zhao, P.; Murshed, M. M.; Alekseev, E. V.; Atuchin, V. V.; Pugachev, A. M.; Gesing, T. M. Synthesis, Structure and Properties of $Na[AsW_2O_9]$. *Mater. Res. Bull.* **2014**, *60*, 258−263.
(56) Atuchin, V. V.; Aleksandrovsky, A. S.; Chimitova, O. D.; Gavrilova, T. A.; Krylov, A. S.; Molokeev, M. S.; Oreshonkov, A. S.; Bazarov, B. G.; Bazarova, J. G. Synthesis and Spectroscopic Properties of Monoclinic α-$Eu_2(MoO_4)_3$. *J. Phys. Chem. C* **2014**, *118*, 15404−15411.
(57) Zinkevich, M. Thermodynamics of Rare Earth Sesquioxides. *Prog. Mater. Sci.* **2007**, *52*, 597−647.
(58) Zhang, P.; Navrotsky, A.; Guo, B.; Kennedy, I.; Clark, A. N.; Lesher, C.; Liu, Q. Y. Energetics of Cubic and Monoclinic Yttrium Oxide Polymorphs: Phase Transitions, Surface Enthalpies, and Stability at the Nanoscale. *J. Phys. Chem. C* **2008**, *112*, 932−938.
(59) Jiang, S.; Liu, J.; Lin, C. L.; Bai, L. G.; Xiao, W. S.; Zhang, Y. F.; Zhang, D. C.; Li, X. D.; Li, Y. C.; Tang, L. G. Pressure-Induced Phase Transition in Cubic Lu_2O_3. *J. Appl. Phys.* **2010**, *108*, 083541.
(60) Levin, I.; Brandon, D. Matestable Alumina Polymorphs: Crystal Structures and Transition Sequences. *J. Am. Ceram. Soc.* **1998**, *81*, 1995−2012.
(61) Yen, F. S.; Wang, M. Y.; Chang, J. L. Temperature Reduction of θ- to α-Phase Transformation Induced by High-Pressure Pretreat-

DOI: 10.1021/acsami.5b08411
ACS Appl. Mater. Interfaces 2015, 7, 26235−26243

ments of Nano-Sized Alumina Powders Derived from Boehmite. *J. Cryst. Growth* **2002**, *236*, 197−209.
(62) Kim, H. N.; Lee, S. K. Effect of Particle Size on Phase Transitions in Metastable Alumina Nanoparticles: A View from High-Resolution Solid-State ^{27}Al NMR Study. *Am. Mineral.* **2013**, *98*, 1198−1210.
(63) Su, L. T.; Tok, A. I. Y.; Boey, F. Y. C.; Zhang, X. H.; Woodhead, J. L.; Summers, C. J. Photoluminescence Phenomena of Ce^{3+}-Doped $Y_3Al_5O_{12}$ Nanophosphors. *J. Appl. Phys.* **2007**, *102*, 083541.
(64) Xiang, W.-D.; Zhao, B.-Y.; Liang, X.-J.; Chen, Z.-P.; Xie, C.-P.; Luo, L.; Zhang, Z.-M.; Zhang, J.-F.; Zhong, J.-S. Packaging Technologies and Luminescence Properties of Ce:YAG Single Crystal for White Light-Emitting Diode. *J. Inorg. Mater.* **2014**, *29*, 614−620.
(65) Arjoca, S.; Villora, E. G.; Inomata, D.; Aoki, K.; Sugahara, Y.; Shimamura, K. Ce:$(Y_{1-x}Lu_x)_3Al_5O_{12}$ Single-Crystal Phosphor Plates for High-Brightness White LEDs/LDs with High-Color Rendering (Ra > 90) and Temperature Stability. *Mater. Res. Express* **2014**, *1*, 025041.
(66) Luo, J.-L.; Wu, Y.-T.; Ren, G.-H. Luminescence Property and Energy Transfer of Ce^{3+}, Eu^{3+} Co-Doped $Lu_3Al_5O_{12}$ Polycrystals. *Wuji Cailiao Xuebao* **2014**, *29*, 1211−1217.
(67) Kichanov, S. E.; Frolova, E. V.; Shevchenko, G. P.; Kozlenko, D. P.; Belushkin, A. V.; Lukin, E. V.; Malashkevich, G. E.; Rakhmanov, S. K.; Glazkov, V. P.; Savenko, B. N. Investigation of Structural Features of the $Y_3Al_5O_{12}$:Ce^{3+}/Lu_2O_3 Crystal Phosphors Formed by the Colloidal Chemical Method. *Phys. Solid State* **2013**, *55*, 813−820.
(68) Ivanovskikh, K. V.; Ogiegło, J. M.; Zych, A.; Ronda, C. R.; Meijerink, A. Luminescence Temperature Quenching for Ce^{3+} and Pr^{3+} *d-f* Emission in YAG and LuAG. *ECS J. Solid State Sci. Technol.* **2013**, *2*, R3148−R3152.
(69) Hamilton, D. S.; Gayen, S. K.; Pogatshnik, G. J.; Ghen, R. D.; Miniscalco, W. J. Optical-Absorption and Photoionization Measurements from the Excited States of Ce^{3+}:$Y_3Al_5O_{12}$. *Phys. Rev. B: Condens. Matter Mater. Phys.* **1989**, *39*, 8807−8815.
(70) Nikl, M.; Yoshikawa, A.; Kamada, K.; Nejezchleb, K.; Stanek, C. R.; Mares, J. A.; Blazek, K. Development of LuAG-based Scintillator Crystals − A Review. *Prog. Cryst. Growth Charact. Mater.* **2013**, *59*, 47−72.
(71) Mullins, W. M.; Averbach, B. L. Bias-Reference X-ray Photoelectron Spectroscopy of Sapphire and Yttrium Aluminum Garnet. *Surf. Sci.* **1988**, *206*, 29−40.
(72) Kaczmarek, S. M.; Sugak, D. J.; Matkovskii, A. O.; Moroz, A.; Kwaśny, M.; Durygin, A. N. Radiation Induced Recharging of Cerium Ions in Nd, Ce:$Y_3Al_5O_{12}$ Single Crystals. *Nucl. Instrum. Methods Phys. Res., Sect. B* **1997**, *132*, 647−652.
(73) Kaczmarek, S. M.; Domianiak-Dzik, G.; Ryba-Romanowski, W.; Kisielewski, J.; Wojtkowska, J. Changes in Optical Properties of Ce:YAG Crystals under Annealing and Irradiation Processing. *Cryst. Res. Technol.* **1999**, *34*, 1031−1036.
(74) Dai, Q. Q.; Duty, C. E.; Hu, M. Z. Semiconductor-Nanocrystals-Gased White Light-Emitting Diodes. *Small* **2010**, *6*, 1577−1588.
(75) Xia, Z. G.; Zhang, Y. Y.; Molokeev, M. S.; Atuchin, V. V. Structural and Luminescence Properties of Yellow-Emitting NaSc-Si_2O_6:Eu^{2+} Phosphors: Eu^{2+} Site Preference Analysis and Generation of Red Emission by Codoping Mn^{2+} for White-Light-Emitting Diode Applications. *J. Phys. Chem. C* **2013**, *117*, 20847−20654.

DOI: 10.1021/acsami.5b08411
ACS Appl. Mater. Interfaces 2015, 7, 26235−26243